Progress In Electromagnetics Research, Vol. 132, 177–198, 2012

SURFACE WAVES RADIATION BY FINITE ARRAYS OF MAGNETOELECTRIC RESONATORS

C. Jouvaud[1, 2, *], A. Ourir[2], and J. de Rosny[2]

[1]CEA, DAM, GRAMAT, F-46500 Gramat, France

[2]Institut Langevin, Université Denis Diderot Paris 7, UMRS CNRS 7587, ESPCI, 10 rue Vauquelin 75231 Paris cedex 05, France

Abstract—We study the propagation of waves on infinite and finite size arrays made of subwavelength magnetoelectric resonators. We propose an analytical study where each magnetoelectric resonator is modelled simultaneously by an electric and a magnetic dipole. We show how near field coupling and wavenumber quantification due to the finite size of the structure induce a frequency splitting of the resonator fundamental mode. We theoretically demonstrate that despite a spatial period of the waves smaller than half wavelength (in vacuum), the structure can efficiently emits radiations. An analytic expression of the Q factor associated to the radiation losses is proposed. To correctly estimate this factor, we show that not only near but also far field interaction terms between the dipoles must to be considered.

1. INTRODUCTION

Interaction of electromagnetic waves with periodic structures of resonant metallic scatterers when these last are separated by less than a fraction of a wavelength is a challenging field. Such structures were first studied in microwave engineering with two-dimensional periodic metallic arrays [1–3] (also known as frequency selective surfaces) and raised significant interests in various fields, such as metallic photonic crystals [4–8], plasmonic devices [9–12] and latter for developing metamaterials [13]. Indeed, metamaterials are composite structures based on periodic arrays of metallic resonators interacting simultaneously with magnetic and electric fields. Many different metallic resonators have been studied such as the well-know split ring resonator (SRR) [10, 13], thin wires [9, 14] or Jerusalem crosses [2], etc..

Received 10 July 2012, Accepted 11 September 2012, Scheduled 27 September 2012

* Corresponding author: Camille Jouvaud (camille.jouvaud@espci.fr).

More recently, metamaterial-like effects have been obtained thanks to hybridization effects between two electrical resonators [15–20].

In 2000, Pendry predicted that a metamaterial with a negative index makes a perfect lens [21]. However, other ways have been proposed to overcome the limit of resolution. Some of them are based on plasmonic-like behaviour of arrays of metallic resonators [8, 22–25]. In [24, 25], they take benefit of the spatio-temporal control of the wavefront to focus electromagnetic pulses on sub-wavelength spots from the far field radiation. The work presented here is directly related to these last works because we provide a simple model of the sub-wavelength waves that propagates along a finite size array of resonators. We also explain how the can emits electromagnetic energy.

Different approaches have been proposed to model and simulate the interaction of wave with resonant inclusions. Among them, we can mention plane wave expansion, finite element method, finite difference time domain method, method of moments (MoM), etc. MoM [26] is especially well suited for periodic arrays of metallic resonators [1, 27]. About ten years ago, a model derived from transmission line theory has also been proposed to describe the propagation of magneto-inductive waves, i.e., surface waves on an array of magnetic resonators [28]. The approach has been validated experimentally [29]. One major advantage of this model consists of providing some straightforward physical interpretations of the results.

Here, we propose to extend the last approach to small metallic resonators that interact simultaneously with the electric and the magnetic field. To that end, like in [30], we assume that a resonator can be approximated as the superposition of an electric and a magnetic dipole. The two dipole moments are driven by the same complex current intensity. Considering infinite arrays of resonators, we work out the relation of dispersion with respect to the direction of propagation. Then we compute the eigen-modes of a finite size array. These modes are interpreted as the splitting of the resonator fundamental mode. We show that the maximum number of resonances is equal to the number of cells. The complex current on each resonator is worked out from the diagonalization of the mutual coupling matrix. To finish with, the radiated fields of the eigenmodes are investigated. We focus on the Q factor due to ohmic and radiative losses. We show that the radiative losses are due to the tiny components of the eigenmodes with a spatial period larger than the wavelength.

In the first part of this article, we present the results of two "numerical experiments" computed with single resonating cells and arrays of 4 by 4 cells. The spectra obtained with 3-gap SRR and 4-gap SRRs provide a basis for discussions. The second part begins with

the derivation of the mutual coupling between electric and magnetic dipoles. Then the system of equations that takes into account all the interactions between every cells is introduced. We show how the relation of dispersion of waves can be deduced from the previous set of equations in case of an infinite array. In a third part, we study finite size arrays of electromagnetic resonators. In the last part, we focus on the losses of such arrays.

2. COUPLING EFFECTS ON ARRAYS OF SUBWAVELENGTH RESONATORS

2.1. Fundamental Mode of Isolated Resonators

The study is focused on arrays of subwavelength electromagnetic resonators. These resonators can interact simultaneously with the electric and magnetic field. Here, we deal with two simple geometries with different symmetries to illustrate the survey. The two structures are multi-gap split ring resonators [31–33]. Fig. 1 shows a schematic view of the two proposed cells and their dimensions. The first one is a square ring with 3 gaps (see Fig. 1(a)) etched on 1 mm-thick epoxy substrate ($\varepsilon = 4$, $\tan\delta = 0.02$). Each gap is at middle of one side. The 3-gap cell is symmetric with respect to plane (Oyz). The second one, shown in Fig. 1(b), is obtained by adding a gap on the fourth side. Therefore, this 4-gap cell is also symmetric with respect to (Oxz) plane. We are going to show that the spectral properties are strongly relied on symmetry. Before studying arrays of cells, we first characterize the electromagnetic response of the individual cells. In

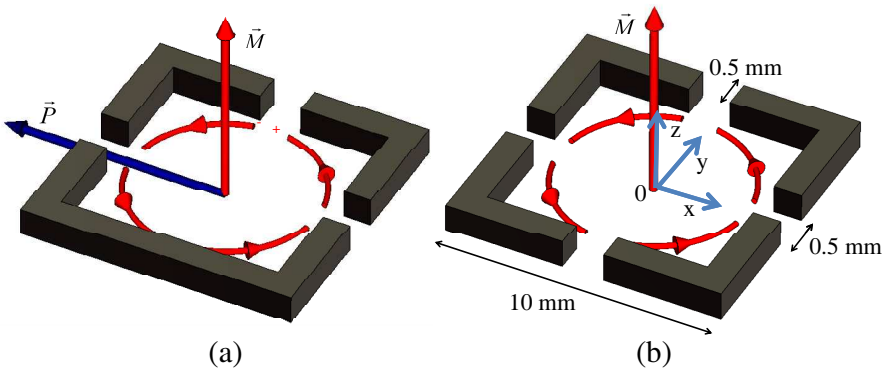

Figure 1. Two resonant metallic cells with two different geometrical symmetries: (a) Is a 3-gap SRR and (b) is a 4-gap SRR.

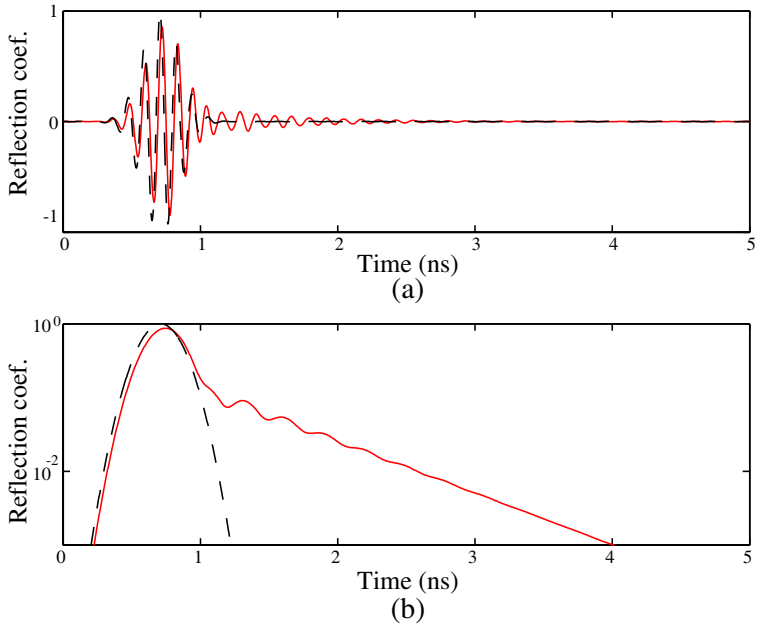

Figure 2. Transient response (continuous red line) of the small loop in front of the 4-gap SRR to a wide-band burst excitation. The burst frequency bandwidth is between 6 and 11 GHz. (a) Show the radio frequency signals and (b) the envelop of the signals.

the following, our developments are sustained with numerical results obtained with a FDTD electromagnetic simulation (CST Computer Simulation Technology AG).

Because we are going to study the response of arrays composed of such cells to a local excitation, we numerically estimate the reflection parameter of a small magnetic antenna, a 3 mm-diameter current loop, placed above the 3-gap and 4-gap cell. The transient response obtained with the 4-gap SRR is shown in Fig. 2. From the Fourier transform of the transient signal, CST works out the reflection coefficient versus frequency. Fig. 3 plots the reflection coefficient for the 3 and 4-gap SRR. The magnetic loop alone does not radiate in this frequency band because its radius is very small compared to the wavelength. Therefore the reflection coefficient is mainly due to the multi-gap SRR. We clearly observe a first strong resonance at 5.5 GHz for the 3-gap cell and at 7.3 GHz for the 4-gap cell. These resonances correspond to the fundamental mode of each cell. Near the resonance, we assume that the multi-gap SRR behaves as a simple resistor-inductor-capacitor

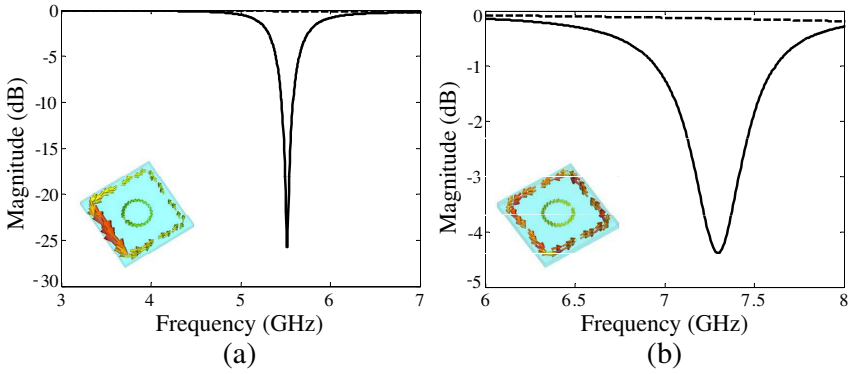

Figure 3. The continuous line is the frequency dependence of the reflection coefficient of a small magnetic loop antenna in front of (a) a single 3-gap SRR and (b) a 4-gap SRR. The dash-line is the reflection coefficient of the small magnetic loop antenna alone. The inset figures represent the current distribution.

circuit. Hence, the resonance frequency ω_0 is then equal to $1/\sqrt{L_s C_s}$ where L_s and C_s are the equivalent inductance and capacitance of the resonator.

Fig. 3 also shows the current distributions at ω_0 for the two cell geometries. For both of them, we observe that the electric current forms a closed loop which induces a magnetic dipole like in a magnetic loop. Due to the flat cell geometry, the magnetic moment is normal to the surface. The origin of the difference between the 3 and 4-gap arrays comes from the symmetry breaking. In both cases, due to the plane geometry, the charge density distribution induces electric dipoles parallel to the substrate. But because 4-gap cells are also symmetric with respect to (Oxz) and (Oyz) planes (see Fig. 1), the charge distribution of the fundamental resonating mode is anti-symmetric with respect to these two last planes. Thus the 4 electric dipoles that are induced between the 4 gaps cancel in pair and the coupling between cells is mainly magnetic. On the contrary three gap cells show a symmetry only with respect to (Oyz) plane. Because the charge density is antisymmetric with respect to this plane but not with respect to (Oxz) plane, it generates a dipole parallel to y-axis.

In the next section, we propose a simple method to model the coupling between two electromagnetic cells based on these observations.

2.2. Mode Splitting in a Finite Array of Resonators

We are interested in the coupling between such cells when they are periodically arranged in a finite array and separated by a distance of about a tenth of a wavelength. To that end, we simulate a structure made of 4 by 4 cells as shown in Fig. 4. For simulations, the distance between the cells is 1 mm. The periodicity of the array is consequently of 11 mm. One cell of the array is excited by a small magnetic loop antenna, whose axis is coincident with the axis of the considered cell. By this way, a normal magnetic field excites the structure. Because of the flat geometry of the structure, the electric field mainly lies in the Oxy plane and the magnetic field is parallel to z-axis. Fig. 4 compares the reflection coefficients of the small magnetic loop antenna when this last is alone and in front of the 3-gap cell array. With the 4 by 4 cell array, several strong resonant frequencies appear. This mode splitting of the fundamental mode is due to the coupling between the 16 cells. These resonances correspond to Fabry-Perot modes. For some of the important dips (resonant modes), we have shown the map of the normal component of the magnetic field in the plane of the structure. To begin, as frequency increases, the complexity of the mode pattern (M_1, M_2, M_3) increases too. For the mode M_4, the spatial fluctuations of the mode pattern is maximum because the current of two adjacent cells are opposite in direction. Then, as the frequency continues to increase, the complexity of the modes M_5, M_6, M_7 decreases. Expressed in terms

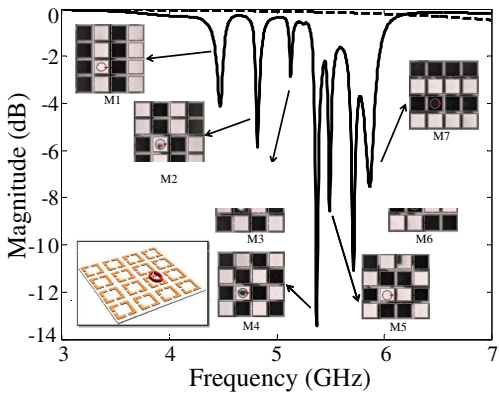

Figure 4. Continuous line is the reflection coefficient of a small magnetic loop in front of a 4 by 4 array of 3-gap SRR (see subfigure). The dash-line is the reflection coefficient of the small magnetic loop alone. The grey level maps correspond to the phase sign of the normal magnetic field distribution at some resonant frequencies.

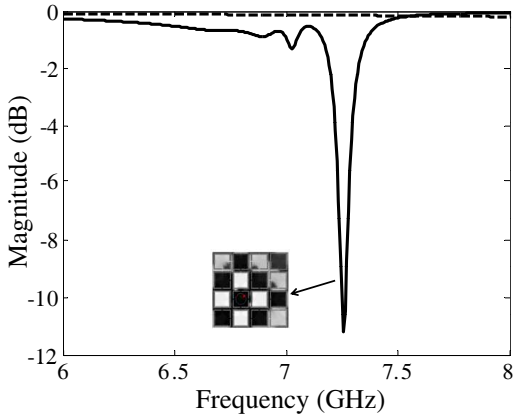

Figure 5. Reflection coefficient of a small magnetic loop in front of a 4 by 4 array of 4-gap SRR (continuous line) and of the small magnetic loop alone (dash-line). The grey level maps correspond to the normal magnetic field distribution at the resonant frequency.

of wavenumber, the Ox and Oy components (k_x, k_y) of modes M_1, M_4 and M_7 are respectively given by $(\frac{\pi}{a}, 0), (\frac{\pi}{a}, \frac{\pi}{a})$ and $(0, \frac{\pi}{a})$ where a is the period of the lattice. Hence, it seems that the coupling between the cells is mainly vertical at low frequency and horizontal at high frequency. This complicated behavior is due to the Oxz symmetry breaking of the 3 gap geometry. Indeed, in case of 4 gaps, only the main resonance M_4 appears (see Fig. 5).

In the next sections, we show that the spectrum behavior is well explained by considering the coupling between electric and magnetic dipoles.

3. THEORY

3.1. Dipole Model for Magnetoelectric Resonators

For thin conductors, the magnetic moment at the center of the structure is given by $1/2 \int I(l)\mathbf{r} \times d\mathbf{l}$ and the electric moment is given by $1/j\omega \int \partial_l I(l)\mathbf{r}d\mathbf{l}$ where $I(l)$ is the current at curvilinear abscissa l. Close to the fundamental resonant frequency, only one degree of freedom is available on the cell, the complex amplitude of the mode or in other words the complex current intensity I. This observation means that the electric and magnetic moments are proportional to I:

$$\mathbf{p} = \frac{dI}{j\omega}\mathbf{u}_d \text{ and } \mathbf{m} \equiv SI\mathbf{u}_m. \tag{1}$$

Constant S is the equivalent surface of the magnetic loop and $\mathbf{u}_m$ its normal direction. As for d, it represents the equivalent length of the dipole and $\mathbf{u}_p$ its direction.

Due to the resonant behavior of the cell, we assume that $\mathbf{m}$ and $\mathbf{p}$ only weakly depend on the frequency and the position of the cell in the structure. The electromotive force (emf) induced by cell #1 onto cell #2 (see Fig. 6) is expressed as the sum of two terms

$$emf_{21} = -j\omega \iint \mathbf{B}_1 . d\mathbf{S}_2 + \oint \mathbf{E}_1 . d\mathbf{l}_2, \tag{2}$$

where the first (respect. second) term is the emf induces by the magnetic dipole (respect. the electric dipole) of cell #1 on cell #2. Fields $\mathbf{E}_1$ and $\mathbf{B}_1$ stand for the electric and magnetic fields, respectively, generated by cell #1 at the position of cell #2. Their expressions are well-known [34] (see (A2) in the appendix). For sake of simplicity, we assume these fields constant over the domains of integration. Consequently, the emf induced by the magnetic induction only depends on the distance between the cells, r. But in case of emf induced by the electric dipole, it also depends on the angle θ (see Fig. 6). This is due to the asymmetry of the cell.

Finally, from (A2) and (2), it comes

$$\begin{aligned} emf_{12}(r,\theta) \;=\; & \frac{I\eta e^{jk_0 r}}{4\pi r^3 k_0} \left[S^2 \left(-jk_0^4 r^2 - k_0 r^3 + jk_0^2 \right) \right. \\ & \left. + d^2 \left(-jk_0^2 r^2 \sin^2(\theta) + [rk_0 - j] \left[3\cos^2(\theta) - 1 \right] \right) \right] \end{aligned} \tag{3}$$

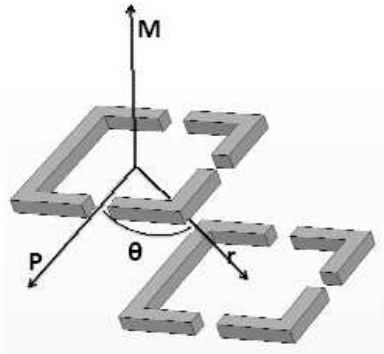

Figure 6. Schematic representation used for the estimation of the interaction between two 3-gap cells. The electric and magnetic moments are shown. The value θ is the angle between the distance vector $\mathbf{r}$ that links the two cells and the electric dipole moment.

The upper and lower limits of the electromotive force are obtained for $\theta = 0$ and $\theta = \pi/2$, respectively.

When $d \geqslant S\omega/c$, the effect of the electric dipole dominates the magnetic one. In such a case and because an electric dipole generate close electric field lines, the sign of the emf goes from positive to negative values when θ increases. In the next sections, we show that this property is fundamental to explain the complex coupling behavior observed in Section 2.2.

3.2. Equation System of Surface Waves

Close to the resonance frequency of one cell, we assume that each cell acts as a simple resonant circuit. Then the self impedance of each cell Z_s is equal to the sum of an inductance $j\omega L_s$, a capacitance $1/j\omega C_s$ and a resistance R_s.

On each resonator, the potential drop due to the resonator is equal to the sum of the emf induced by the other cells (Kirchhoff's voltage law). It gives rise to a set of N equations where N is the number of cells

$$\left(j\omega L_s + \frac{1}{j\omega C_s} + R_s\right) I(l,m) + \sum_{l' \neq l, m' \neq m} Z_m\left(l'-l, m'-m\right) I\left(l', m'\right) = 0. \quad (4)$$

The first term is the electric potential difference induced by the resonator itself and the second one describes the mutual coupling between the cells. Eq. (4) is the fundamental set of equations to model the coupling between the cells. In the next sections, we deduce from this relation the relation of dispersion of an infinite size array of resonators and also the discrete spectrum for a finite size system.

3.3. Relation of Dispersion of an Infinite Size Array

In case of an infinite array, it can be shown that a plane wave is solution of (4). Replacing $I(l,m)$ by $I(k_x,k_y)\exp(-i[k_x a l + k_y a m])$ and considering only the near field interaction (i.e., the mutual impedance) with the four closest neighbors leads to an explicit dispersion relation:

$$\omega = \omega_0 \sqrt{\frac{1 + C_s C_m^{-1}[-2\cos(k_x a) + 4\cos(k_y a)]}{1 - L_m L_s^{-1}[2\cos(k_x a) + 2\cos(k_y a)]}}. \quad (5)$$

When C_m is very large and L_m very small, there is no coupling and the angular frequency is equal to ω_0. When $C_m \gg C_s$, the inductive coupling dominate and Eq. (5) is the dispersion relation of the magneto-inductive waves [28, 29, 35]. Note that this expression can be also worked out from the Lagrangian formalism [30, 36].

For a square flat loop with dimensions given in Fig. 1, the equivalent electric model elements are evaluated using [37] (p. 245). The self impedance is about 2.4 nH when the current is assumed as uniform[†]. This value is overestimate because in our case the current is not uniform around the loop. An inductance of 0.5 nH (respect. 0.4 nH) is coherent with the simulation result for the 3-gap (respect. 4-gap) cells. A capacitance of about 1.6 pF (respect. about 0.8 pF) is then deduced from the resonance frequency.

From dipole approximation, the mutual capacitance C_m and inductance L_m are given by $4\pi\epsilon_0 a^3/d^2$ and $\mu_0 S^2/4\pi a^3$, respectively. From the double integral Neumann formula, a more exact estimation of L_m can be obtained. Both approaches give a mutual inductance of roughly 0.1 pH. The dipole length d is approximately given by the size of the gap for the 3-gap cell and it is equal to zero in case of the 4 gaps because there is no electric moment.

From these values, the dispersion relations on 4 major directions of the reciprocal lattice of the square lattice are plotted in Fig. 7(a) and Fig. 7(b) for the 3 and 4 gap SRRs, respectively. In case of the 3-gap SRR, the dispersion relation is not the same in the ΓXM and $\Gamma X'M$ directions. From (5), we can easily find that the coupling induce a frequency span between $\omega_0(1-6C_sC_m^{-1})/(1+4L_mL_s^{-1})$ and $\omega_0(1+6C_sC_m^{-1})/(1-4L_mL_s^{-1})$. This two extrema are in accordance with the frequency splitting observed in Fig. 4.

The slope of the dispersion relation of the array made of 4-gap cells is negative (backward waves) because the magnetic coupling between two parallel loops is negative. The slope sign of the 3-gap dispersion relation is either positive or negative. Along the ΓX axis, the wave is vector is parallel to the electrical dipoles. The dispersion curve is therefore positive because the coupling of aligned dipoles is positive. Along the $\Gamma X'$ axis, the wave vector is perpendicular and the coupling negative.

Nevertheless, the spectra observed in Figs. 4 and 5 can only be explained by considering a finite size array.

3.4. Extraction of the Eigenmodes for a Finite Size Array

For finite size array, the sum in (4) is finite and there is no simple analytical solution like for the infinite array. In such a case, it is helpful to express the linear set of equations into a single matrix equation:

$$\mathbf{Z}_s\mathbf{I} + \mathbf{Z}_m\mathbf{I} = \mathbf{S}, \tag{6}$$

[†] Self impedance of a squared loop with sides a and wire radius b is given by $2\mu_0\frac{a}{\pi}\left[\ln\left(\frac{a}{b}\right) - 0.774\right]$.

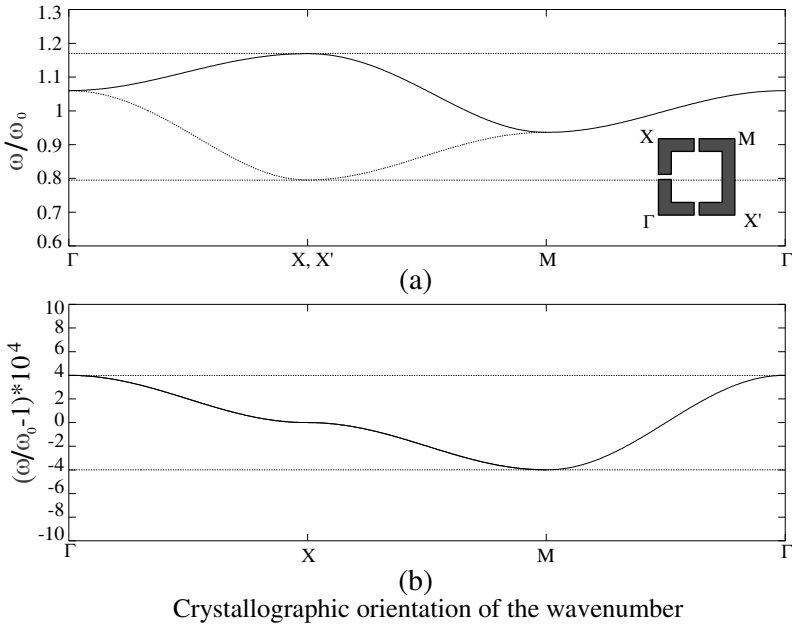

Figure 7. Dispersion relations for two arrays of (a) 3-gap cells and of (b) 4-gap cells. The dispersion relation is plotted on 4 major axis of the Brillouin zone (see inset). The continuous line follows the ΓXM path and the dashed line follows the $\Gamma X'M$. The dashed lines shows the minimum and maximum values (see text).

where $\mathbf{I}$ and $\mathbf{S}$ are the current vector and the source vector with N complex elements. This approach has been also applied in [28, 35]. The number of columns and raws of the self-impedance matrix $\mathbf{Z}_s$ and the mutual impedance matrix $\mathbf{Z}_m$ is N *by* N. The i-th element of the vector $\mathbf{I}$ is the complex amplitude of the current at i-th cell. The vector $\mathbf{S}$ models the effect of the source term (the small loop) which generates an electromotive force on the cells. Matrix $\mathbf{Z}_s$ is the product of the eye (unitary) matrix times $(j\omega L_s + 1/j\omega C_s + R_s)$. Finally the $(l,\ l')$ element of $\mathbf{Z}_m$ is equal to the mutual impedance between the cell l and l'. In case of a rectangular array of M_x rows and M_y columns of resonators, the simpliest manner to index the resonator at position i_x and i_y (i_x and i_y are expressed in the coordinate system Oxy) is $l = (i_x - 1)M_y + i_y$. The inversion of Eq. (6) yields to estimate the current $\mathbf{I}$. In the next section, we diagonalize the mutual impedance matrix to inverse Eq. (6).

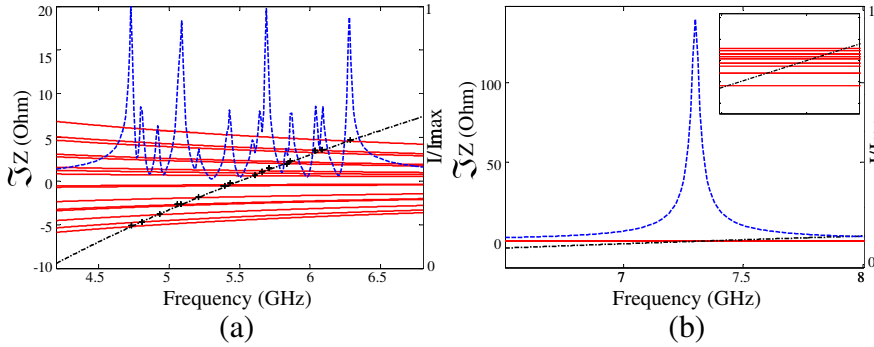

Figure 8. The continuous red lines and the dash-dotted back line represent the imaginary part of the eigenvalues and of the self impedance, respectively. The dashed blue line is the module of the current at one particular cell. (a) Plot is obtained for a 3-gap array and (b) plot for a 4-gap array. Each array is composed of 4 by 4 elements.

3.4.1. Inversion from Eigendecomposition

Thanks to reciprocity, the matrix $\mathbf{Z}_m$ is symmetrical, we can perform its spectral decomposition which can be expressed as

$$\mathbf{Z}_m = \sum \mathbf{U}_{\mathrm{n}}^{\mathrm{H}} \lambda_n \mathbf{U}_n, \tag{7}$$

where λ_n are the complex eigenvalues and $\mathbf{U}_n$ the associated complex eigenvectors. Vectors $\mathbf{U}_n$ which form an orthonormal basis are also the eigenvectors of $\mathbf{Z}_s$ because this last is proportional to the eye matrix. Consequently, the current distribution vector can be deduced from

$$\mathbf{I} = \sum \frac{\mathbf{U}_n^H \mathbf{U}_n}{\lambda_n + Z_s} \mathbf{S}. \tag{8}$$

A resonance occurs at the poles of the previous equation, i.e., when at least one denominator of the sum is null. Because the real part of $\lambda_n + Z_s$ is always positive and almost constant, the minimum is reached when its imaginary part is null. Thus, the n-th resonance angular frequency ω_n is worked out from the equation $\Im\lambda_n = -\Im Z_s$[‡]. It may happen that there is no solution to the previous equation which means that the nth mode cannot be excited. This approach is numerically validated using the two arrays of 4 by 4 cells introduced in Subsection 2.2. In this simulations, the real part of the self-impedance is set to 0.07Ω that is the radiative resistance of a small circular loop of

[‡] $\Im X$ is the imaginary part of X.

same radius than our multigap SRRs [34]. However, this value is very approximate because the 3-gap and 4-gap geometries are more complex than a simple small circular loop. This real part of the self impedance has to be seen as the combined effect of the radiative and the ohmic losses of a cell. At this stage, the effects of these two losses on the intensity spectrum are identical. Fig. 8 plots the current amplitude at one cell using Eq. (6). The same figure also plots the frequency dependence of the 16 eigenvalues of the mutual impedance matrix and $-Z_s$. As expected, we observe that all resonances occur when the imaginary part of λ_n and $-Z_s$ are crossing together. However we are going to see in the last part of this article that when the ohmic loss are small compared to the radiative losses, it is not sufficient to only take into account the near field and the closest neighborhoods to estimate the radiated power, i.e., the Q factor, of a finite size array.

3.4.2. Eigenmodes of a Finite Size Array

Because the mutual impedance only depends on the difference of positions between two resonators, the complex intensity at column i_x and row i_y of the (n_x, n_y) eigenvector is approximately given by

$$U^{(n_x,n_y)}_{(i_x-1)M_y+i_y} \propto I_0 \sin(k_x^{n_x} a i_x) \sin(k_y^{n_y} a i_y) \tag{9}$$

with $k_x^{n_x} = n_x\pi/a(M_x+1)$ and $k_y = n_y\pi/a(M_y+1)$ for $(n_x, n_y)\epsilon[1, M_x-1]\times[1, M_y-1]$. Larger the array, the more exact the approximation is. The quantified values of $k_x^{n_x}$ and $k_y^{n_y}$ are obtained from the condition that the current is null outside the array [28]. Therefore, there are $M_x \times M_y$ eigenmodes. Assuming only the effect of the closest neighbors, there exists an analytical expression of the eigenvalue of the (n_x, n_y) mode:

$$\lambda_{(n_x,n_y)} = 2Z_x \cos\left(\frac{\pi n_x}{M_x-1}\right) + 2Z_y \cos\left(\frac{\pi n_y}{M_y-1}\right), \tag{10}$$

where Z_x and Z_y are the mutual impedance on x and y axis.

In Fig. 4, the coupling between 3-gap SRR generates about ten resonances. The 16 resonances are not observed because some of them are only weakly excited by the source. Moreover the resonance frequencies of some of them are too close from each other to be resolved. For the 4-gap SRR, $Z_x = Z_y$. In such case, when we switch n_x and n_y, the same eigenvalue is obtained which means that for a square array of cells, there are about half the number of resonant frequencies compared to the non-degenerated case. Nevertheless, here we only observe one resonance frequency because the magnetic coupling is not strong enough to induce a significant splitting of the fundamental

resonance. In that case, the normal magnetic field pattern presented in Fig. 5 results from a superposition of all the modes.

4. RADIATED FIELD OF A FINITE SIZE ARRAY OF RESONATORS

With the same approach, the radiation pattern can be easily deduced from the currents distribution. Fig. 9 shows four calculated radiation patterns for different eigenmodes of the 3-gap SRR array. Each pattern results from complex interferences between the wave radiated by each magnetoelectric dipole. Each radiation pattern is characterized by a Q factor.

Theoretical evaluation of the radiated field by a finite size array of resonators is a tedious problem. Indeed, in case of a large array of cells, when we assume that there is no ohmic loss, eigen-modes are not

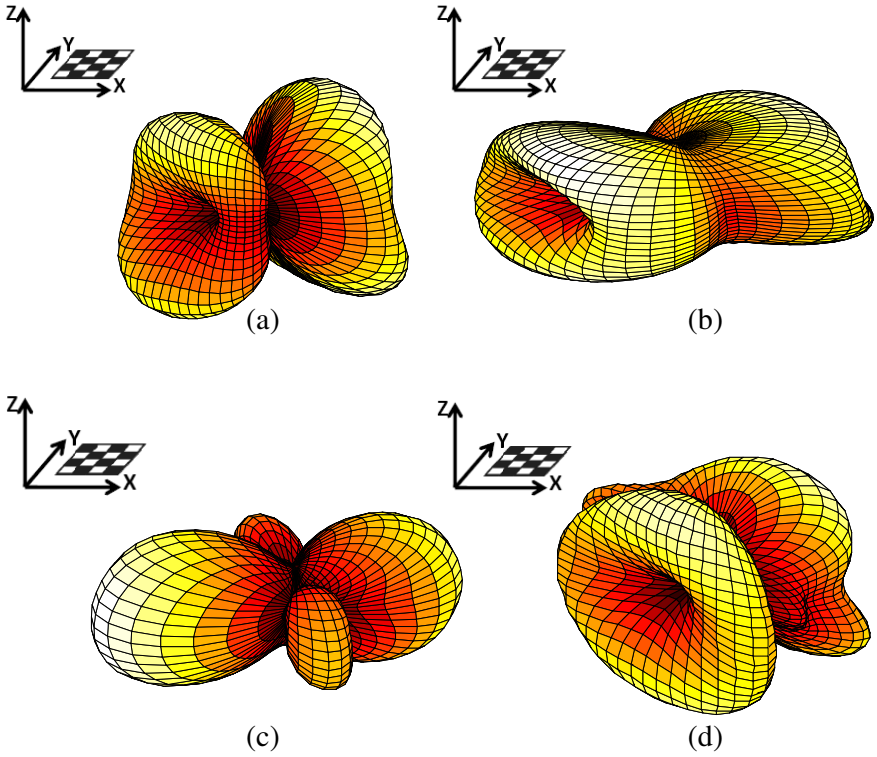

Figure 9. Radiation patterns for the 4 by 4 array of 3-gap SRR at frequencies: (a) 4.47 GHz, (b) 5.37 GHz, (c) 5.49 GHz, (d) 5.62 GHz.

attenuated because the period of the field is smaller than λ_0 and there is no way for the wave to be converted into propagative one. However, in case of a finite size array, the extension of the cosine function is now bounded by a rectangular function. The Fourier transform of this eigen-mode contains now some components with spatial periods that are equal or larger than the wavelength. Hence, a 'subwavelength' eigenmode can radiate because of these components.

To quantify this effect, we compute the quality factor of each individual resonance. As stated, a resonance at ω_n occurs when $\Im\lambda_n + \Im Z_s \approx 0$. Around this resonance frequency, we assume that $\lambda_n + Z_s$ can be linearized. Then (Eq. (8)) can be approximated by

$$\mathbf{I} = \sum \frac{\mathbf{U}_n^H \mathbf{U}_n}{\Re(\lambda'_n)\left(1 + j\frac{\omega-\omega_n}{\Re(\lambda'_n)}\frac{\partial \Im\lambda'_n}{\partial\omega}\right)}\mathbf{S}, \tag{11}$$

where $\lambda'_n = \lambda_n + Z_s$. The λ'_n are the eigenvalues of a mutual impedance matrix plus the self impedance matrix. From the previous expression, we immediately deduce the Q_n factor of nth resonance

$$Q_n = \frac{\partial \Im\lambda'_n}{\partial\omega}\frac{\omega_n}{\Re\lambda'_n}. \tag{12}$$

Hence, Q_n factor is driven by λ'_n. For a linear (1D) array of resonators, the n-th eigen-values can be deduced from the nth eigen-vectors by

$$\lambda'_{n_x} = \sum_{l_x, m_x=1}^{M_x} Z(a[l_x - m_x]) U^*_{n_x}(l_x) U_{n_x}(m_x), \tag{13}$$

where $Z(x)$ is the mutual impedance function matrix between two resonators that are away from a distance x and a the period of the array. By definition, $Z(0)$ is the self impedance matrix. Replacing, the mutual impedance function Z and U_{n_x} by their Fourier transform $\tilde{Z}$ and $\tilde{U}_{n_x}$ respectively, the previous expression becomes

$$\lambda'_{n_x} = \frac{1}{2\pi}\int_{k_x=-\infty}^{\infty} \tilde{Z}(k_x)\left|\tilde{U}_{n_x}(k_x a)\right|^2 dk_x. \tag{14}$$

This expression can be straightforwardly generalized to 2D arrays

$$\lambda'_{n_x,n_y} = \frac{1}{2\pi}\int_{k_x,k_y=-\infty}^{\infty}\left[\tilde{Z}(k_x,k_y)\right]\left|\tilde{U}_{n_x,n_y}(k_x a, k_y a)\right|^2 dk_x dk_y. \tag{15}$$

The Q factor is the ratio between $\partial \Im \lambda'_{n_x}/\partial\omega$ and $\Re\lambda'_{n_x}$. Assuming a sufficiently large array, one can deduce from (14) or (15) that $\Im\lambda'_{n_x}$ does not depend strongly on the array size. The resonances of the array occur when the frequency obeys to the relation of dispersion given by Eq. (5) with $k_x^{n_x} = n_x\pi/a(M_x+1)$. At these frequencies $\Im\lambda'_{n_x}$ is equal to zero. In the same way, $\partial\Im\lambda'_n/\partial\omega$ only weakly depends on the array size. But it is not anymore the case for the real part of λ'_{n_x}.

Indeed, Fig. 10 plots the Fourier transform of the mutual impedance matrix between two dipoles. We clearly observe that the real part of the Fourier transform of the impedance does not include evanescent components. In other words, for an infinite array without losses, the wave on the array does not radiate. Indeed, in such a case the eigenvectors are sine functions of wavenumber k_x and its Fourier transform is a Dirac centered on k_x. When k_x is larger than ω/c, the eigen-value is purely imaginary. For $k_x > \omega/c$, the only way to dump the wave is to add ohmic loss. However, for a finite size system, we observe that the Fourier transform of the eigenmodes is not a Dirac, but a sinc-like function. From (15), we note that the finite size effect does not drastically modify the value of the imaginary part of the eigenvalue which is approximately the value of the Fourier transform of the imaginary part of the mutual impedance at k_x. But now, instead being zero between $-k_0$ and k_0, the Fourier transform of the eigen-modes shows some ripples. Consequently the real part of the eigenmode is weak but larger than 0. In that case, the high Q_n factor is due to the wave radiation.

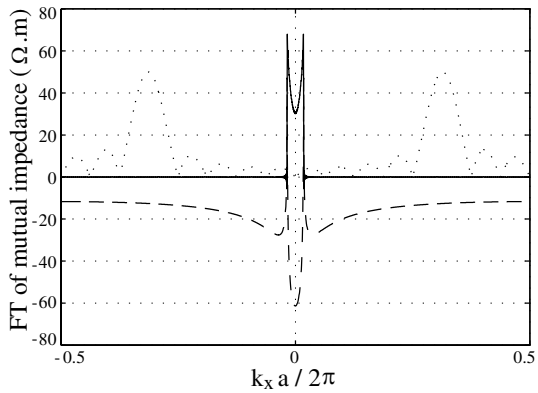

Figure 10. Real (–) and imaginary part (-.) of the Fourier transform of the mutual impedance between two electrical dipoles. The continuous line is the Fourier transform of one eigen-mode.

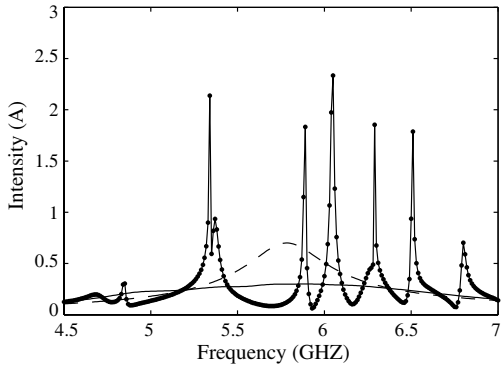

Figure 11. Intensity level on one resonator for an array of 4 by 4 resonators without ohmic loss. The continuous line is obtained when only the reactive near field of the closest neighbors is taken into account. The dashed line results from the effect of the closest neighbors including all interaction terms in Eq. (A5). Finally, the dotted line is obtained when the neighbors and the interaction terms contribute all together.

5. DISCUSSION

A question that constantly arises is the number of cells that should be taken into account to correctly estimate coupling effects on an array of resonant cells. If it is sufficient to take into account the closest neighbors to predict the basic properties of an array of cells, it is not anymore the case when we are interested in the losses due to radiation for a finite size system. Indeed, in the previous part, we have shown that the radiation can be deduced from the Fourier transform of the mutual impedance between cells. This last is given by a continuous integral of dyadic Green's functions times the imaginary unit. Because, it is well-known that the Fourier Transform of the imaginary part of the Dyadic Green's is zero for a wavevector that is larger than k_0, it is also the case of the real part of the Fourier transform of the mutual impedance. Hence, the radiation is due to a global effect on the array that involves all cells. Contrary to ohmic loss, this effect is not local and cannot be correctly described by taking into account only the near field effect and the radiation resistance of the self impedance. This is confirmed in Fig. 11 where the array does not show resonances when only the closest neighbors are considered in the mutual impedance. This intensity enhancement at the resonance frequency of poorly radiating modes is very similar to the Purcell's effect [38] as explained in [24, 39].

6. CONCLUSION

We developed a model for infinite and finite size arrays of electric and magnetic resonators that are separated by less than a wavelength. Based on this approach, on one side, it is explained why the resonance frequency for a finite size system is essentially governed by the dispersion relation of an infinite size array. But on the other side, it is shown that the finite size of the array induces the mode splitting and radiation efficiency. With the proposed model, we have estimated the Q factor associated with the radiation losses and we have shown that all the resonators contribute to the radiated power. This conclusion is fundamental to understand the radiation efficiency of 'metalenses'.

ACKNOWLEDGMENT

We gratefully acknowledge the financial support of the French government-funded technological research organization CEA/DAM. This work has been also supported by the French National Agency (ANR) with the grant OPTRANS (number 2010 BLAN 0124 04).

APPENDIX A. COMPLETE EXPRESSION OF THE MUTUAL COUPLING

The complete expression of the electric and magnetic field generated by an electric and a magnetic dipole are given by

$$\begin{aligned}\mathbf{E} &= \frac{e^{jk_0r}}{4\pi r\epsilon_0}\left[\left(jk_0+\frac{1}{r}\right)\left[\frac{3(\mathbf{u_r}\cdot\mathbf{p})\mathbf{u_r}-\mathbf{p}}{r}\right]\right.\\ &\left.+k_0^2\mathbf{u}_r\times(\mathbf{p}\times\mathbf{u_r})+j\frac{k_0}{c_0}\left(jk_0+\frac{1}{r}\right)(\mathbf{u_r}\times\mathbf{m})\right], \qquad \text{(A1)}\\ \mathbf{B} &= \frac{\mu_0 e^{jk_0r}}{4\pi r}\left[\left(jk_0+\frac{1}{r}\right)\left[\frac{3(\mathbf{u_r}\cdot\mathbf{m})\mathbf{u_r}-\mathbf{m}}{r}\right]\right.\\ &\left.+k_0^2\mathbf{u_r}\times(\mathbf{m}\times\mathbf{u_r})+j\omega\left(jk_0-\frac{1}{r}\right)(\mathbf{p}\times\mathbf{u_r})\right]. \qquad \text{(A2)}\end{aligned}$$

With the geometrical configuration defined in Fig. 6, the previous expressions become

$$\begin{aligned}\mathbf{E} &= \frac{I\eta e^{jk_0r}}{4\pi r}\left[d\left(1-\frac{j}{k_0r}\right)\left[\frac{3\cos(\theta)\mathbf{u_r}-\mathbf{u}_d}{r}\right]\right.\\ &\left.-jdk_0\left(\mathbf{u}_d-\cos(\theta)\mathbf{u}_r\right)-k_0S\left(-k_0+\frac{j}{r}\right)(\mathbf{u}_\theta)\right], \qquad \text{(A3)}\end{aligned}$$

$$\mathbf{B} = \frac{Ie^{jk_0r}\mu_0}{4\pi r}\left[-S\left(jk_0+\frac{1}{r}\right)\frac{\mathbf{u}_m}{r}+Sk_0^2\mathbf{u}_m + \left(jk_0+\frac{1}{r}\right)d\sin(\theta)\mathbf{u}_m\right]. \quad \text{(A4)}$$

The mutual impedance is deduced from Eq. (2)

$$Z_m(r) = \frac{-I\eta e^{jk_0r}}{4\pi r^3 k_0}\left[S^2\left(-jk_0^4r^2-k_0r^3+jk_0^2\right) + d^2\left(-jk_0^2r^2\sin^2(\theta)+[rk_0-j]\left[3\cos^2(\theta)-1\right]\right)\right]. \quad \text{(A5)}$$

It is assumed that the fields $\mathbf{E}_1$ and $\mathbf{B}_1$ are constant over the integration domain.

REFERENCES

1. Montgomery, J., "Scattering by an infinite periodic array of thin conductors on a dielectric sheet," *IEEE Transactions on Antennas and Propagation*, Vol. 23, 70–75, Jan. 1975.
2. Tsao, C.-H. and R. Mittra, "Spectral-domain analysis of frequency selective surfaces comprised of periodic arrays of cross dipoles and Jerusalem crosses," *IEEE Transactions on Antennas and Propagation*, Vol. 32, 478–486, May 1984.
3. Zarrillo, G. and K. Aguiar, "Closed-form low frequency solutions for electromagnetic waves through a frequency selective surface," *IEEE Transactions on Antennas and Propagation*, Vol. 35, 1406–1417, Dec. 1987.
4. Smith, D. R., S. Schultz, N. Kroll, M. Sigalas, K. M. Ho, and C. M. Soukoulis, "Experimental and theoretical results for a two-dimensional metal photonic band-gap cavity," *Applied Physics Letters*, Vol. 65, No. 5, 645–647, 1994.
5. Sigalas, M. M., C. T. Chan, K. M. Ho, and C. M. Soukoulis, "Metallic photonic band-gap materials," *Phys. Rev. B*, Vol. 52, 11744–11751, Oct. 1995.
6. Suzuki, T. and P. K. L. Yu, "Dispersion relation at point l in the photonic band structure of the face-centered-cubic lattice with active or conductive dielectric media," *J. Opt. Soc. Am. B*, Vol. 12, 583–591, Apr. 1995.
7. Sievenpiper, D. F., M. E. Sickmiller, and E. Yablonovitch, "3d wire mesh photonic crystals," *Phys. Rev. Lett.*, Vol. 76, 2480–2483, Apr. 1996.
8. Maier, S. A., P. G. Kik, H. A. Atwater, S. Meltzer, E. Harel, B. E. Koel, and A. A. G. Requicha, "Local detection of

electromagnetic energy transport below the diffraction limit in metal nanoparticle plasmon waveguides," *Nat. Mater.*, Vol. 2, 229–232, Apr. 2003.

9. Pendry, J. B., A. J. Holden, W. J. Stewart, and I. Youngs, "Extremely low frequency plasmons in metallic mesostructures," *Phys. Rev. Lett.*, Vol. 76, 4773–4776, Jun. 1996.
10. Smith, D. R., D. C. Vier, W. Padilla, S. C. Nemat-Nasser, and S. Schultz, "Loop-wire medium for investigating plasmons at microwave frequencies," *Applied Physics Letters*, Vol. 75, No. 10, 1425–1427, 1999.
11. Maier, S. A., M. L. Brongersma, and H. A. Atwater, "Electromagnetic energy transport along arrays of closely spaced metal rods as an analogue to plasmonic devices," *Applied Physics Letters*, Vol. 78, No. 1, 16–18, 2001.
12. Maier, S. A., P. G. Kik, and H. A. Atwater, "Observation of coupled plasmon-polariton modes in au nanoparticle chain waveguides of different lengths: Estimation of waveguide loss," *Applied Physics Letters*, Vol. 81, No. 9, 1714–1716, 2002.
13. Smith, D. R., W. J. Padilla, D. C. Vier, S. C. Nemat-Nasser, and S. Schultz, "Composite medium with simultaneously negative permeability and permittivity," *Phys. Rev. Lett.*, Vol. 84, 4184–4187, May 2000.
14. Guida, G., D. Maystre, G. Tayeb, and P. Vincent, "Mean-field theory of two-dimensional metallic photonic crystals," *J. Opt. Soc. Am. B*, Vol. 15, 2308–2315, Aug. 1998.
15. Abdeddaim, R., A. Ourir, and J. de Rosny, "Realizing a negative index metamaterial by controlling hybridization of trapped modes," *Phys. Rev. B*, Vol. 83, 033101, Jan. 2011.
16. Ourir, A., R. Abdeddaim, and J. de Rosny, "Double-t metamaterial for parallel and normal transverse electric incident waves," *Optics Letters*, Vol. 36, 1527–1529, May 2011.
17. Podolskiy, V. A., A. K. Sarychev, and V. M. Shalaev, "Plasmon modes in metal nanowires and left-handed materials," *Journal of Nonlinear Optical Physics & Materials*, Vol. 11, No. 1, 65–74, 2002.
18. Zhang, S., W. Fan, N. C. Panoiu, K. J. Malloy, R. M. Osgood, and S. R. J. Brueck, "Experimental demonstration of nearinfrared negative-index metamaterials," *Phys. Rev. Lett.*, Vol. 95, 137404, Sep. 2005.
19. Dolling, G., C. Enkrich, M. Wegener, J. F. Zhou, C. M. Soukoulis, and S. Linden, "Cut-wire pairs and plate pairs as magnetic atoms

for optical metamaterials," *Optics Letters*, Vol. 30, 3198–3200, Dec. 2005.

20. Linden, S., M. Decker, and M. Wegener, "Model system for a one-dimensional magnetic photonic crystal," *Phys. Rev. Lett.*, Vol. 97, 083902, Aug. 2006.
21. Pendry, J. B., "Negative refraction makes a perfect lens," *Phys. Rev. Lett.*, Vol. 85, 3966–3969, Oct. 2000.
22. Alù, A. and N. Engheta, "Theory of linear chains of metamaterial/plasmonic particles as subdiffraction optical nanotransmission lines," *Phys. Rev. B*, Vol. 74, 205436, Nov. 2006.
23. Shvets, G., S. Trendafilov, J. B. Pendry, and A. Sarychev, "Guiding, focusing, and sensing on the subwavelength scale using metallic wire arrays," *Phys. Rev. Lett.*, Vol. 99, 053903, Aug. 2007.
24. Lemoult, F., G. Lerosey, J. de Rosny, and M. Fink, "Resonant metalenses for breaking the diffraction barrier," *Phys. Rev. Lett.*, Vol. 104, 203901, May 2010.
25. Li, X. and M. I. Stockman, "Highly efficient spatiotemporal coherent control in nanoplasmonics on a nanometer-femtosecond scale by time reversal," *Phys. Rev. B*, Vol. 77, 195109, May 2008.
26. Harrington, R., "Matrix methods for field problems," *Proceedings of the IEEE*, Vol. 55, 136–149, Feb. 1967.
27. Chen, C.-C., "Scattering by a two-dimensional periodic array of conducting plates," *IEEE Transactions on Antennas and Propagation*, Vol. 18, 660–665, Sep. 1970.
28. Shamonina, E., V. A. Kalinin, K. H. Ringhofer, and L. Solymar, "Magnetoinductive waves in one, two, and three dimensions," *Journal of Applied Physics*, Vol. 92, 6252–6261, Nov. 2002.
29. Shamonina, E. and L. Solymar, "Magneto-inductive waves supported by metamaterial elements: Components for a one-dimensional waveguide," *Journal of Physics D-applied Physics*, Vol. 37, Int. Phys. Dielectr. Grp., Feb. 2004.
30. Liu, N., H. Liu, S. Zhu, and H. Giessen, "Stereometamaterials," *Nature Photonics*, Vol. 3, 157–162, Mar. 2009.
31. Zhou, J., T. Koschny, M. Kafesaki, E. N. Economou, J. B. Pendry, and C. M. Soukoulis, "Saturation of the magnetic response of split-ring resonators at optical frequencies," *Phys. Rev. Lett.*, Vol. 95, 223902, Nov. 2005.
32. Aydin, K., I. Bulu, K. Guven, M. Kafesaki, C. M. Soukoulis, and E. Ozbay, "Investigation of magnetic resonances for different split-ring resonator parameters and designs," *New Journal of Physics*, Vol. 7, No. 1, 168, 2005.

33. Penciu, R. S., K. Aydin, M. Kafesaki, T. Koschny, E. Ozbay, E. N. Economou, and C. M. Soukoulis, "Multi-gap individual and coupled split-ring resonator structures," *Optics Express*, Vol. 16, 18131–18144, Oct. 2008.
34. Orfanidis, S. J., *Electromagnetic Waves and Antennas*, Electronic book, Chap. 16, 655, Aug. 2010, http://www.ece.rutgers.edu/ orfanidi/ewa/.
35. Sydoruk, O., O. Zhuromskyy, A. Radkovskaya, E. Shamonina, and L. Solymar, *Theory and Phenomena of Metamaterials*, Metamaterials Handbook, Chap. 7, 36-1–36-13, CRC Press/Taylor & Francis, 2009.
36. Liu, H., D. A. Genov, D. M. Wu, Y. M. Liu, Z. W. Liu, C. Sun, S. N. Zhu, and X. Zhang, "Magnetic plasmon hybridization and optical activity at optical frequencies in metallic nanostructures," *Phys. Rev. B*, Vol. 76, 073101, Aug. 2007.
37. Balanis, C., *Antenna Theory: Analysis and Design/Constantine A. Balanis*, J. Wiley, New York, 1982.
38. Purcell, E. M., "Spontaneous emission probabilities at radio frequencies," *Proceedings of the American Physical Society*, Vol. 69, 674–674, American Physical Society, Apr. 1946.
39. Lemoult, F., M. Fink, and G. Lerosey, "Revisiting the wire medium: An ideal resonant metalens," *Waves in Random and Complex Media*, Vol. 21, No. 4, 591–613, 2011.